SI traceable calibration of an instrumented indentation sensor spring constant using electrostatic force

Koo-Hyun Chung, Stefan Scholz, Gordon A. Shaw, John A. Kramar, and Jon R. Pratt
Manufacturing Engineering Laboratory, National Institute of Standards and Technology, Gaithersburg, Maryland 20899, USA

(Received 20 February 2008; accepted 1 September 2008; published online 22 September 2008)

We present a measurement scheme for creating reference electrostatic forces that are traceable to the International System of Units. This scheme yields reference forces suitable for calibrating the force sensitivity of instrumented indentation machines and atomic force microscopes. Forces between 10 and 200 μN were created and expressed in terms of the voltage, length, and capacitance between a pair of interacting electrodes. The electrodes comprised an electrically conductive sphere mounted as a tip on an instrumented indentation sensor, and a planar counterelectrode fixed to a sample stage in close proximity to the sphere. For comparison, we applied mechanical forces of similar magnitudes, first using deadweights and then using a reference force sensor. The deflection of the sensor due to the various applied forces was measured using an interferometer. A spring constant for the sensor was computed from the observed records of force versus displacement. Each procedure yielded a relative standard uncertainty of approximately 1%; however, the electrostatic technique is scalable and could provide traceable reference forces as small as a few hundred piconewtons, a range far below anything yet achieved using deadweights. © *2008 American Institute of Physics.*
[DOI: 10.1063/1.2987695]

I. INTRODUCTION

Test instruments such as atomic force microscopes (AFMs) and instrumented indentation machines are widely used for the physical characterization of materials and devices when high spatial resolution and small feature sizes are of interest. AFMs are primarily used in imaging modes to provide topographic information, but they can also record the force interaction between the cantilever sensor tip and a sample. At the atomic scale, this means that AFMs probe diverse phenomena ranging from, for example, the mechanical properties of collagen,[1] to the complex force dependent structure of DNA,[2] to the spin state of a single electron.[3] Similarly, at the scale of thin film organic and inorganic structures, instrumented indenters record the force necessary to press a sharp tip into a submicrometer size material sample. These instruments routinely measure mechanical properties such as elastic modulus and hardness.[4–6] In both AFMs and instrumented indenters, measuring the force interaction between the tip and surface involves measuring the deflection of a spring suspension. In the case of an AFM, the force sensor itself is a microfabricated cantilever that functions as a passive mechanical sensor. In an instrumented indenter, an external force (typically electrostatic or electromagnetic) drives the spring suspension to which the indenter tip is attached. Users interested in small force measurements must therefore determine the suspension spring constant, or otherwise calibrate this deflection as a force. Recent attention has focused on the goal of absolute accuracy and traceability for these calibrations.[7–15]

The most direct and accurately known reference force is a mass suspended in the earth's gravitational field, otherwise known as deadweight force. However, relative uncertainties in small masses accumulate as one subdivides from the kilogram, so that a traceable deadweight force in the range of several nanonewtons might have an uncertainty on the same order as the measurement.[7] Issues of uncertainty aside, deadweights are not always practical, since the size of the deadweight for small forces can be unwieldy when compared to the size of the sensor, particularly for AFMs. In an effort to derive an alternative to deadweights, the National Institute of Standards and Technology (NIST) has developed the electrostatic force balance (EFB),[8] which provides a means to directly compare mechanical forces to known electrostatic forces using an electromechanical balance system. This balance has been used to calibrate an array of reference cantilevers[9] and a piezoresistive cantilever that functions as a force transfer standard.[10,11] Outside NIST, a microelectromechanical device[12] has been demonstrated that could traceably calibrate a reference spring for use in AFM calibration using measurements of current and velocity, and a quantum based realization of the piconewton has been proposed based on superconducting electromagnetics.[13] Approaches based on the calibration of piezoresistive sensors using high-resolution mass balances[14,15] have also been demonstrated but these do not explicitly realize an alternative force, since they continue to rely on mass for traceability.

In this paper, we apply concepts developed for the EFB to the problem of applying traceable reference forces directly to a force sensor, rather than through a reference artifact, such as the previously mentioned cantilevers. Here, SI traceable electrostatic forces are quantitatively determined by direct measurement of the capacitance gradient between a test sensor load button and a fixed electrode. To validate this measurement scheme, the spring constant k of a commercially manufactured force sensor (normal force transducer, Hysitron, Inc., Minneapolis, Minnesota[16]) was measured us-

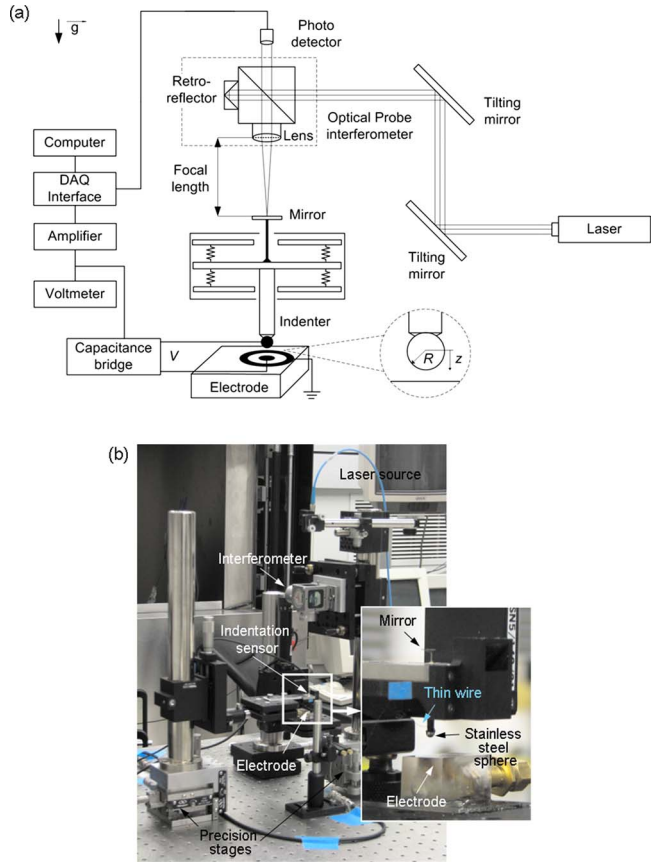

FIG. 1. (Color online) (a) Schematic and (b) photograph of experimental setup.

ing force and displacement data. The estimate based on application of electrostatic force is $k=k_e$, which we compare to two additional independent, traceable techniques; $k=k_r$ is based on applying forces by pressing against a deadweight calibrated reference sensor, while $k=k_w$ is based on applying forces by hanging deadweights directly on the indentation sensor. The spring and the measurement of its displacement were consistent in all three cases, so that variation in the computed values of stiffness should be a direct indication of systematic differences between the force generation schemes.

Sections II through IV describe the general experimental setup and procedures, the results, and the uncertainties for each of the force calibration methods. We finish by drawing some conclusions about the potential application of the electrostatic technique to smaller force and size scales. Our results suggest that the electrostatic force method could be scaled to smaller values than either of the other two methods, while maintaining traceability.

II. CALIBRATION BY ELECTROSTATICS

A. Principles of a SI traceable electrostatic reference force

We seek to apply calculable electrostatic forces to a grounded electrode mounted on a compliant force sensor. A proposed arrangement is illustrated schematically in Fig. 1(a), where electrostatic forces act on a spherical electrode suspended from a uniaxial spring of stiffness k that follows Hooke's law, so the deflection of the spring is proportional to the applied force. The geometry of this capacitor is variable along a single coordinate corresponding to constrained motion along path s. The electrostatic force on the suspended electrode can be expressed mathematically as

$$F_e = \frac{1}{2}\frac{dC}{ds}(U^2), \tag{1}$$

where F_e is the electrostatic force along the path s of the variable capacitor, dC/ds is the gradient of capacitance along this direction, with ds being the differential displacement of the moving electrode along s, dC the corresponding differential change in capacitance, and U an electrical potential between the two electrodes.

The experimental problem reduces to accurately measuring the capacitance gradient dC/ds and the electrical potential U. The gradient may be approximated to within a few tenths of a percent by measuring capacitance as a function of the displacement z, which is the motion of the electrode measured by a laser interferometer which has been aligned to the sensor axis to within less than a few tenths of a radian. This measurement of the gradient dC/dz can be done traceably by using a reference capacitor and a capacitance bridge to record the value of C, and an interferometer referenced to a known wavelength of light to record changes in the displacement dz of the sphere with respect to the flat, as the suspended electrode is deflected by, for example, applying different electrical potentials to the fixed electrode.

The applied electrical potential U may be measured traceably using a calibrated voltmeter; however, surface potentials and time-varying voltages, such as the capacitance bridge excitation, must also be accounted for. The total electrical potential between the electrodes is

$$U = V_{\mathrm{dc}} + V_{\mathrm{ac}} \sin \omega t + V_s, \tag{2}$$

where V_{dc} is the measured applied voltage, V_{ac} is the amplitude of the bridge excitation, having angular frequency ω, and V_s is the surface potential, which arises because of differences in the work functions of the electrode surfaces (contact potentials between the voltmeter and the electrodes are also included in this term). Squaring this total potential and substituting in Eq. (1) we find

$$F_e = \frac{1}{2}\frac{dC}{dz}\left[(V_{\mathrm{dc}} + V_s)^2 + \frac{V_{\mathrm{ac}}^2}{2} + 2(V_{\mathrm{dc}} + V_s)V_{\mathrm{ac}} \sin \omega t - \frac{V_{\mathrm{ac}}^2}{2}\cos 2\omega t\right], \tag{3}$$

where it is clear that the electrical force has both static and dynamic components. The time-varying components of the electrical force can be averaged over an integer number of bridge cycles, so that their contributions to the determination of a static electrical force are zero. Furthermore, by computing the change in average force with application or change of V_{dc}, the effect of $V_{\mathrm{ac}}^2/2$ can be made negligible for the case where dC/dz is a weak function of the electrode separation, so that Eq. (3) reduces to the following expression:

$$\Delta F_e = \frac{1}{2}\frac{dC}{dz}(V_{\mathrm{dc}}^2 + 2V_{\mathrm{dc}}V_s). \tag{4}$$

Dynamic forces resulting from the bridge excitation still present some problems for weak suspensions during the gradient measurement, since the dynamic force can cause the electrode to oscillate significantly while trying to measure its capacitance. With care, a combination of bridge excitation level and frequency can usually be found where the suspended electrode motion is negligible.

V_s must be determined in order to apply Eq. (4), and we observe that working from expressions for both the sum and difference of the forces resulting from V_{dc}'s of opposite polarities, the following quadratic equation is obtained:

$$V_s = |V_{\mathrm{dc}}|\frac{(z_+^{1/2} - z_-^{1/2})^2}{z_+ - z_-}, \tag{5}$$

where z_+ is the deflection of the sensor for a positive voltage and z_- is the corresponding deflection for the same negative voltage. Therefore, by measuring the deflections of the indentation sensor when positive and negative potentials are applied, the surface potential can be estimated, provided dC/dz is approximately uniform over the deflection range from z_+ to z_-.

As a matter of practicality, we restrict ourselves to a capacitor that has cylindrical symmetry, so that electrical forces arising along the x-axis and y-axis should cancel, and not contribute to the balance of forces acting on the capacitor. Expecting deviations from perfect symmetry, we further rely on the mechanical constraint of the suspension to reject contributions to the force from the inevitable, unmeasured, off-axis gradients. In other words, Eq. (4) assumes either perfectly symmetric electrode geometry, or a suspension that is free from cross-axis coupling of forces and moments to motions along z. Furthermore, it is important either that the capacitor electrodes are electrically isolated from the suspension, or that the suspension itself is cylindrically symmetric about the measurement axis. We chose the former approach, working with a suspension that was electrically isolated and shielded from the sphere by a ground plane.

B. Experimental details

A commercially manufactured force sensor designed to measure force and displacement during instrumented indentation was used as the test sensor. The sensor was selected because it provided a convenient, flexure spring, constrained to motion along a vertical axis. The embedded sensing and actuation elements were not used. Experiments consisted of applying known forces to the sensor load button, recording the resulting displacement of this button, and curve fitting the results to arrive at the effective sensor spring constant. The main physical elements of the experiment included the test indentation sensor with mounting and alignment stages, a displacement measuring interferometer with optics and stages for alignment, and various devices for applying the forces to the sensor load button along a prescribed measurement axis. The entire physical setup could be isolated in a Plexiglas box to minimize the effects of air currents on measurements. The major components are shown in Fig. 1, with the Plexiglas box removed for clarity.

The stiffness of the sensor will depend on the orientation of its measurement axis with respect to the force vector. Consistent coordinates for each experiment were established by keeping both the displacement measurement axis z and the sensor axis s aligned to gravity as follows. A Zygo optical probe laser interferometer[17] was used to measure the sensor deflection z in a direction normal to the measurement mirror which was affixed atop the indentation sensor, providing a traceable measurement of the deflection of the sensor that was linked to a wavelength standard with relative uncertainty less than a few parts in 10^6. The measurement mirror was a flat piece of chrome-coated coverslip glass ($3\times3\times0.5$ mm^3) affixed to the indenter tip holder on the top side of the sensor opposite the indenter tip, as in Fig. 1. The top, flat surface of the sensor mount was taken as normal to the sensor axis s, as is the manufacturer's practice, and oriented to gravity using a bubble level. The measurement mirror was attached to the sensor using epoxy, and this mirror was clamped to a level reference surface during curing of the epoxy so that its surface remained normal to within 9 mrad of arc.

As shown in Fig. 1, a stainless steel sphere of radius $R=1$ mm was attached to the indentation sensor's tip holder (side opposite of the measurement mirror) with epoxy. A flexible copper wire of 50 μm diameter connected the sphere electrically to a coaxial cable rigidly fixed to the sensor body. The combined added weight (mirror and sphere) was 1.2 mN causing a static deflection of about 8 μm. For the counterelectrode, a coaxial cable that is smaller than the sphere was used to minimize the effect of background capacitance. A semirigid coaxial cable was mounted in a polycarbonate block, and the copper center conductor (1 mm diameter), Teflon insulation, and rigid shield conductor were polished to create a smooth, planar electrode. This flat electrode was positioned below the sphere [see inset of Fig. 1(b)] with the plane of this electrode aligned to gravity using a bubble level. The sphere was centered above the flat electrode by maximizing the capacitance at a fixed separation. The field was considered symmetric after this alignment, and the direction of electrostatic force was then assumed to be normal to the fixed electrode surface.

Capacitance was measured using an Andeen-Hagerling 2500-A capacitance bridge (AH bridge) that included an internal reference capacitor traceable to NIST standard reference capacitors. The measurement used a three terminal arrangement[18] where the sphere was held as a virtual ground, and bias voltages were applied through the bridge while simultaneously recording the capacitance. A relative standard uncertainty, $u(C_i)/|C_i|$ in the capacitance transfer of the AH bridge was estimated to be 5×10^{-6} based on manufacturer's data.[18] An Agilent 3458a voltmeter was used to measure the voltage V_{dc}. This voltmeter had been calibrated against Zener and resistive divider standards at NIST that are traceable to a SI realization of the volt achieved using a Josephson junction array. A relative standard uncertainty $u(V_i)/|V_i|$ of voltage transfer is estimated to be 1.55×10^{-6}.[19]

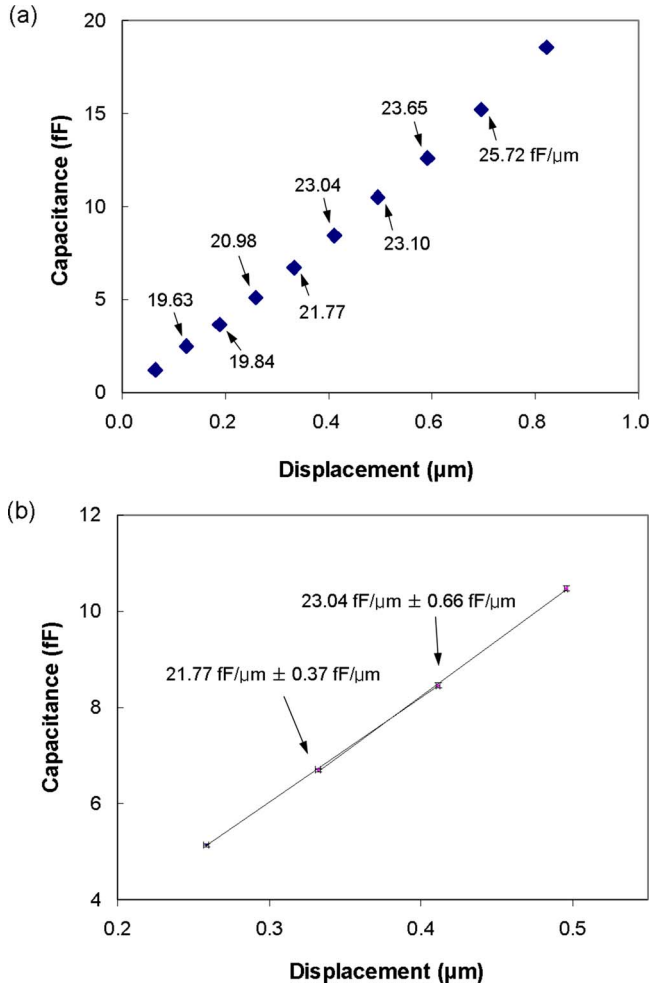

FIG. 2. (Color online) (a) Full and (b) local plots of capacitance vs displacement, including calculated capacitance gradients, for a representative electrostatic force experiment.

For direct electrostatic calibration of the indentation sensor, stepwise voltages were applied in ten increments up to 100 V to produce attractive forces between the sphere and flat electrodes. Each of these force increments consisted of two measurement periods. The first period was characterized by zero applied potential and the second period by a positive polarity voltage step. The final 100 V increment was followed by a return to zero applied potential, so that each application of electrostatic force was bracketed by periods of zero potential, providing a means to monitor drift in the baseline conditions. To gain more accurate measurement of capacitance, the bridge frequency and voltage were set to 1 kHz and 3 V, respectively. No significant oscillation in the position of the indentation sensor was observed as the result of the bridge excitation voltage during experiments. Average values of C, z, and V_{dc} were measured and recorded during each period, with the capacitance bridge set for a time constant of ~4 s, the voltmeter set to average for 120 power line cycles (2 s), and z computed from 2 s of interferometer data sampled at 100 kHz. These average values were sampled five times at nominally four second intervals by a personal computer (PC)-based data acquisition system, and the average and standard deviation of these five values recorded for each period. We assumed that the drifts in these averaged values were linear with respect to time during the force application, and compensated the incremental changes accordingly when the data were analyzed after the experiment. The entire series of potentials was repeated for seven trials, with the steel sphere realigned to the flat electrode between each complete trial as necessary. In four of the seven trials, the voltage increments included a third measurement period where a negative polarity voltage step was added so that V_s could be computed from Eq. (5).

C. Experimental results

A typical plot of capacitance versus displacement through a full electrostatic force trial is shown in Fig. 2(a). It can be seen that dC/dz increases significantly as the gap between the sphere and flat electrode decreases (larger displacement on the plot corresponds to decreasing gap). The functional relationship between C and z was expected to be nonlinear and similar to published results obtained using the method of images for a sphere-on-flat capacitor.[20,21] However, attempts to fit the data to such models proved unsatisfactory, and we conclude that our capacitor geometry deviates too significantly from that assumed in the model (e.g., in our case, the sphere diameter is greater than the flat electrode diameter). As a compromise approach, approximate values of dC/dz were obtained through local linear curve fits. For the ten increments in force, eight linear dC/dz values were estimated from three point line fits to the data as outlined below:

$$C = f(z) = \begin{bmatrix} \left.\frac{dC}{dz}\right|_2 z + b_2 & z_1 \le z \le z_3 \\ \left.\frac{dC}{dz}\right|_3 z + b_3 & z_2 \le z \le z_4 \\ \vdots & \vdots \\ \left.\frac{dC}{dz}\right|_9 z + b_9 & z_8 \le z \le z_{10}, \end{bmatrix} \tag{6}$$

where b is the intercept for linear curve fitting. Representative slopes for adjacent segments were 23.0 ± 0.7 fF/μm for the interval 0.33 μm$< z <$ 0.50 μm and 21.8 ± 0.4 fF/μm for 0.26 μm$< z <$ 0.41 μm, respectively, as shown in Fig. 2(b). The stated uncertainty is an estimate based on procedures outlined in Ref. 22 for computing the uncertainty of a linear curve fit when both the dependent and independent variables possess significant measurement uncertainties.

Negative voltage increments were included in four of the trials for determination of the surface potential. The difference between $z+$ and $z-$ varied from 10 to 45 nm as the magnitude of the applied voltage was increased from 30.5 to 96.4 V. The surface potential was estimated at each of the eight force increments within a trial where an estimate of dC/dz had been made (e.g., all but the first and last force increments). An average surface potential between the sphere and the flat electrode was then computed for each trial. These average values ranged from 1.18 to 2.05 V. We

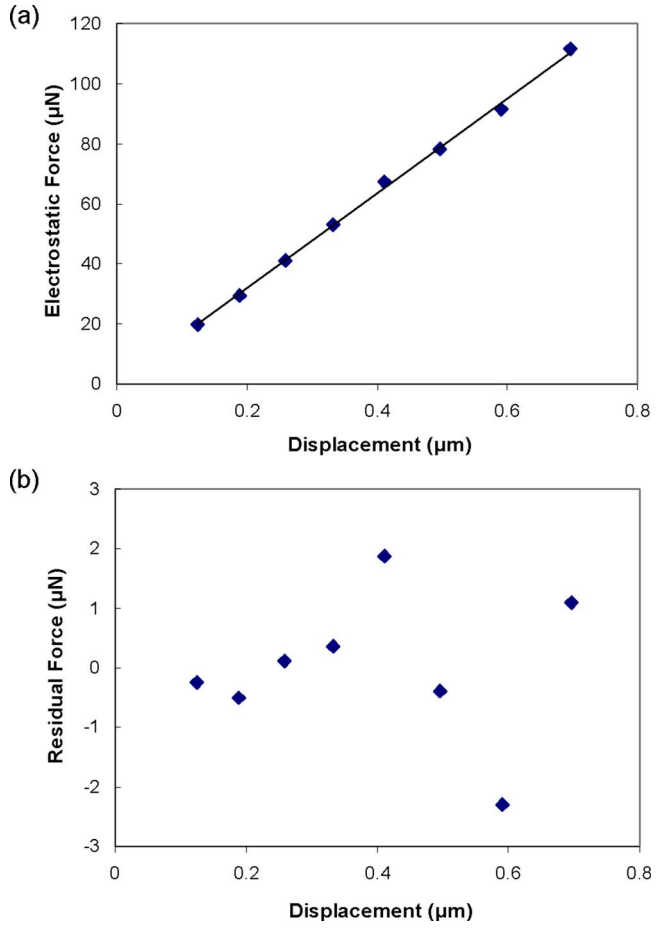

FIG. 3. (Color online) Representative electrostatic calibration: (a) spring constant plot and (b) residual forces after least-squares fitting to a straight line.

note that the statistical variation of the estimates within a trial was typically 7%, which is less than the trial to trial variation.

The surface potential is due, in part, to the difference between the work functions of stainless steel (sphere) and copper (flat electrode), which should be consistent from trial to trial. However, surface oxides and adsorbed contamination layers can contribute substantially to the surface potential,[23,24] neither of which was controlled in these experiments. Furthermore, the sphere was brought into contact with the flat electrode at the start of each experiment as part of a procedure used to estimate the gap. We suspect that this may have caused significant variation in the surface contamination, contributing to the trial to trial variation. No physical damage of the electrode was observable using an optical microscope.

A typical plot of the calculated applied electrostatic force with respect to the measured displacement of the indentation sensor is given in Fig. 3(a). The maximum applied electrostatic force for the seven experiments ranged from 62.3 to 112.0 μN and the maximum deflection of the indenter ranged from 397 to 696 nm. A high degree of linearity ($R^2=0.9985$) between the electrostatic force and deflection is observed, and the plot of residual forces in Fig. 3(b) appears random and free of any deterministic trends. Finally, the average spring constant, k_e obtained from the seven experiments was 158 N/m with a standard deviation of 2 N/m (relative standard deviation: 1×10^{-2}).

D. Uncertainty analysis

The interferometer was aligned to gravity and to the measurement axis of the sensor within an angle θ_{zs} of 9 mrad, contributing a relative uncertainty of 4×10^{-5} due to the cosine of the angle. This and the relative uncertainty in the wavelength, which is less than a part in 10^6, are the dominant type *B* uncertainties of the displacement measurement (see Ref. 25 for a discussion of type *A* versus type *B* measurement uncertainty). We estimate that vibrations of the measurement mirror with respect to the reference mirror on the beam splitter, turbulence, and polarization mixing effects lead to variations of individual displacement measurements on the order of 10^{-8} m. This type *A* uncertainty clearly dominates, since the total displacement measured was on the order of 5×10^{-7} m.

The applied electrostatic force along the sensor axis is

$$\Delta F_e = \frac{1}{2}\frac{dC}{dz}(V_{\mathrm{dc}}^2 + 2V_{\mathrm{dc}}V_s)\cos\,\theta_{es}\,\cos\,\theta_{zs}, \tag{7}$$

where θ_{es} is the angle between the sensor axis and the normal projected from the fixed, flat electrode. The angle θ_{es} was indeterminate but estimated to be within 5 mrad. Neglecting this term may lead to an overstatement of the relative force by at most two parts in 10^5. Other type *B* contributions, such as the uncertainties associated with the transfer of the volt and farad were similarly small and contributed little to the overall relative uncertainty beyond a few parts in 10^5. Very conservatively we estimate the total type *B* contributions to the relative standard uncertainty to be 5×10^{-5}. With regard to type *A* contributions, the standard deviation of typical V_{dc} measurements was on the order of 10 mV, V_s on the order of 0.4 V, and dC/dz on the order of 0.5 fF/μm. Type *A* uncertainty of a force determination is then estimated by summing the component uncertainties in quadrature, premultiplying each term by its proper weight, or sensitivity coefficient.[25] Taking both types *A* and *B* uncertainties into account and summing in quadrature, the combined relative uncertainty in force is written:

$$\frac{dF}{|F|} = \sqrt{\left[2\frac{(V_{\mathrm{dc}}+V_s)u(V_{\mathrm{dc}})}{V_{\mathrm{dc}}^2+2V_sV_{\mathrm{dc}}}\right]^2 + \left[2\frac{u(V_s)}{V_{\mathrm{dc}}+2V_s}\right]^2 + \left[\frac{u(dC/dz)}{dC/dz}\right]^2 + 2.5\times10^{-9}}, \tag{8}$$

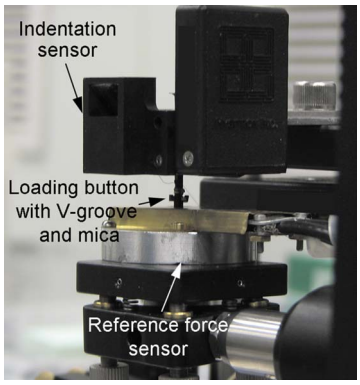

FIG. 4. (Color online) Experimental setup for calibration using the reference force sensor.

where $u(V_{dc})$, $u(V_s)$, and $u(dC/dz)$ are simply the previously quoted values for the standard deviations of the respective variables. The uncertainties at minimum force (13.2 μN) and maximum force (115 μN) were 0.2 and 3.5 μN, respectively.

Type *A* uncertainty of the spring constant was estimated using the relative standard deviation among the seven k_e values that were obtained by least-squares curve fitting of each force displacement curve. This relative standard deviation is 1×10^{-2}, as we reported in the results section. Type *B* contributors to the uncertainty include the wavelength of light, transfer of the electrical units, and the alignment, none of which exceeds a relative uncertainty of a few parts in 10^5 and, even in aggregate, are negligible compared to type *A* uncertainty. The combined relative uncertainty is thus 1×10^{-2}.

III. CALIBRATION BY REFERENCE FORCE SENSOR

A. Experimental details

For measurement of the indentation sensor using a reference force sensor, the experiment was set up as illustrated in Fig. 4. The base of a reference sensor was mounted flush to an actuated stage, the top of which was aligned to gravity using a bubble level. We assumed that the stage translation was free of rotations within our measurement uncertainty. The force readout of the reference sensor is capacitive and was measured using the same bridge employed for the electrostatic experiments. For displacement measurements, the same interferometer setup was used.

The reference force sensor of Fig. 4 was calibrated with relative standard uncertainties of less than a percent using traceable deadweights which were placed on it using an automated system and procedures described in Ref. 26. The masses ranged from 0.5 to 20 mg, and were chosen to cover forces similar in range to the electrostatic calibration. Once calibrated, the reference sensor was placed beneath the indentation sensor, aligned to gravity, and the entire experiment closed up in the isolation chamber. The experimental setup was allowed to equilibrate for several hours. A precision motion stage and a piezoelectric actuator were used to translate the reference sensor into contact with the spherical indenter. A piece of mica that was mounted on the center of the reference sensor's load button provided a smooth and flat location for contact with the stainless steel sphere.

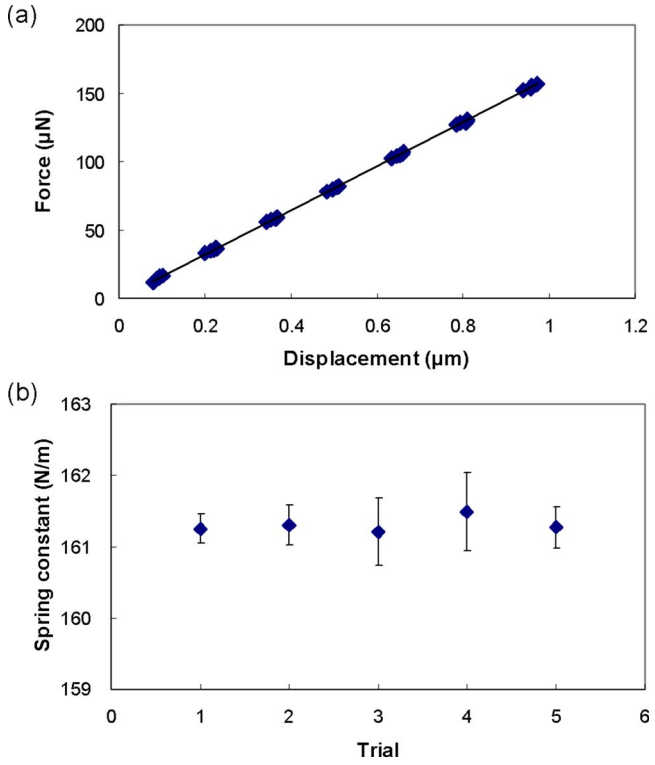

FIG. 5. (Color online) (a) Representative plot of a single trial and (b) spring constants k_r determined using the reference force sensor.

Seven linear stepwise deflections of the indenter spring were produced using the piezoactuator moving the reference sensor. These deflections ranged from 0.1 to 1 μm as measured by the interferometer. The actuator tended to creep during the measurements, therefore, in order to monitor and subtract this drift, the reference sensor was pulled away between each force increment, allowing the sensors to return to their initial out-of-contact conditions. Five measurements of the force and position were collected at each step at ~4 s time intervals. Five trials were carried out using the procedure above with a PC-based data acquisition and control system.

B. Experimental results

As a first basis of comparison to the electrostatic results, data from the reference force sensor experiment are given in Fig. 5. Forces ranging from 4.45 to 175.3 μN were applied to the indentation sensor using the reference sensor. It can be seen that the creep of the piezoactuator manifests itself as a general drift in the recorded force and displacement for a given increment. However, the deflection measured by the interferometer and the force from the reference sensor were gathered simultaneously, so that the data simply drifts along the straight line corresponding to the indentation sensor's linear force displacement behavior, as in Fig. 5(a). The spring constant k_r, along with its standard deviation obtained from five trials, is given in Fig. 5(b). The average value of the spring constant was 161.3 N/m with a standard deviation of 0.1 N/m (relative standard deviation: 7×10^{-4}).

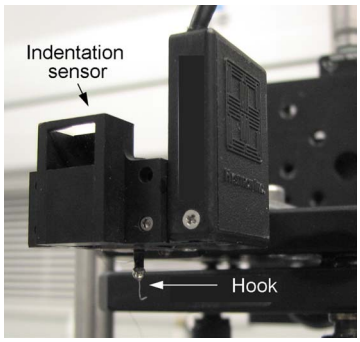

FIG. 6. (Color online) Experimental setup for calibration by deadweight.

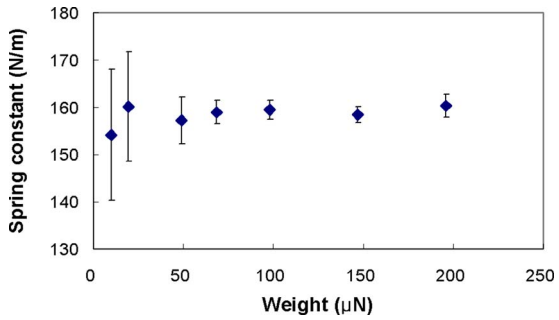

FIG. 7. (Color online) Indentation sensor spring constant calibration results k_w using deadweights.

C. Uncertainty analysis

The relative uncertainty of the force readout from the reference force sensor was determined from the uncertainties of masses, buoyancy, gravity; and cosine error of alignment during deadweight calibration, and is 2×10^{-3}. Details of a similar uncertainty analysis are described in Ref. 26·

The indentation sensor spring constant determined from the reference force sensor experiment is

$$k_r = \frac{f(C)}{z}\cos\,\theta_{rs}\cos\,\theta_{zs}, \tag{9}$$

where $f(C)$ is the force readout from the reference sensor and θ_{rs} is the angle between the indentation sensor axis and the reference force sensor axis. θ_{rs} was estimated to be within 4 mrad, which gives a relative uncertainty of 2×10^{-5} (type *B*). The uncertainties of alignment are negligible compared to the reference sensor's calibration uncertainty.

The relative combined uncertainty of k_r is thus equal to type *A* uncertainty from the multiple curve fits, or 0.1 N/m (relative uncertainty: 7×10^{-4}), combined with the uncertainty of the reference sensor calibration. Summing these two contributions yields a combined relative uncertainty for k_r of 2×10^{-3}.

IV. CALIBRATION BY DEADWEIGHT

A. Experimental details

After completing the electrostatic and reference force sensor based experiments, an additional wire hook was attached to the center of the indentation sensor's stainless steel sphere with epoxy as shown in Fig. 6, which illustrates the setup for the deadweight force experiment. The hook enabled steel wire deadweights to be hung from the bottom of the steel sphere. The interferometer setup for measuring sensor displacements was the same as for the previous calibration methods.

Stainless steel wire masses from 1 to 20 mg, calibrated by the NIST mass group, were used as deadweights. Deadweights were applied and removed manually without the Plexiglas isolation chamber. Each deadweight force application was repeated ten times and the average spring deflection recorded.

B. Experimental results

Results of the spring constant calibration of the indentation sensor by deadweights are shown in Fig. 7. The statistical variations of the computed spring constants were relatively high for the 1 and 2 mg deadweights, although the mean values appear consistent with the other evaluations. Nevertheless, we felt the signal to noise ratio in this force range was unacceptably small and determined that the mean value of the spring constant of the indentation sensor k_w was 159 N/m with a standard deviation of 1 N/m (relative standard deviation: 7×10^{-3}) using only the higher force data.

C. Uncertainty analysis

The uncertainties of the masses used for deadweights were between 2×10^{-3} and 3×10^{-3} mg as determined by the NIST mass group, which leads to maximum relative uncertainties in deadweight forces of 4×10^{-4}, since the local value of gravity was known with a relative uncertainty of better than 1×10^{-6}.

The indentation sensor spring constant determined from the deadweight force experiment is

$$k_w = \frac{\mathrm{mg}}{z}\left(1-\frac{\rho_{\mathrm{air}}}{\rho_{\mathrm{mass}}}\right)\cos\,\theta_{gs}\cos\,\theta_{zs}, \tag{10}$$

where m is the mass of the deadweight, g is the acceleration due to gravity (9.8010 $\mathrm{m/s^2}$), θ_{gs} is the angle between the gravitational and the indentation sensor axis, ρ_{air} is the air density, and ρ_{mass} is the density of the weight. θ_{gs} was estimated to be within 3 mrad, and the ratio of $\rho_{\mathrm{air}}/\rho_{\mathrm{mass}}$ (buoyancy) in the laboratory was determined to be 1.5×10^{-5}.

We conclude that type *B* uncertainties of these corrections to the deadweight force are negligible. Uncertainty in the determination of the spring constant from deadweight loading was dominated by type *A* uncertainty due to variations in the measured spring deflections, which was dominated by vibration noise. The combined relative standard uncertainty is 7×10^{-3}, which is simply the relative standard deviation of the spring constants determined using deadweights between 50 and 200 μN.

V. DISCUSSION

Spring constants obtained from the three different calibration methods are summarized in Table I. All estimates of the spring constant agree within the expanded uncertain-

TABLE I. Spring constant of the indentation sensor measured by three different methods.

Calibration method	Spring constant (N/m)	Uncertainty (N/m)	
		Standard uncertainty	Expanded uncertainty [coverage factor of 2 (Ref. 25)]
Electrostatic, k_e	158	2	4
Reference force sensor, k_r	161.3	0.3	0.6
Deadweight, k_w	159	1	2

ties. The spring constant obtained using the reference force sensor, where the indenter spring was constrained due to contact forces, is slightly larger than the other values, but still falls within the expanded uncertainty, which bounds a 95% confidence interval (i.e., coverage factor of 2) around the electrostatic or deadweight determinations. Nevertheless, this result does provide some evidence that contact between the indentation sensor and a surface can raise the apparent stiffness of the device due to the additional constraint, and certainly warrants further investigation. The agreement among the various spring constant determinations provides confidence that our assumptions about the direction of the electrostatic force, that were based on arguments of physical symmetry in the electrode pair, are valid, at least at the relative uncertainty level of a percent or two.

The uncertainty expressed by Eq. (8) reveals that the accuracy of electrostatic forces achieved when attempting smaller voltage increments depends on the ability to experimentally identify the surface potential V_s. Hypothetically, if we set V_{dc} to be 1 V and all the other values are maintained as in the present experiment, the relative uncertainty on the 10 nN force that would be realized would be 20%. It is important to keep in mind that the rather large uncertainty claimed in our estimate of V_s $(1.65 \pm 0.4$ V) takes into account the variations that were observed between trials (differing experimental setups), and that within any particular trial the estimated relative uncertainty in V_s was on the order of 7%. Thus, for a specific experimental setup, we can produce electrostatic forces on the order of tens of nanonewtons with a relative uncertainty on the order of 6%.

The need for nanonewton-level calibration of indentation sensors as well as of AFM probes is increasing. The electrostatic force approach is scalable to these force levels, and could be applicable to, e.g., conductive colloidal probes used in adhesion studies with AFM, where such forces are quite common. These systems are difficult to calibrate, owing to the sphere appended to the end of the AFM probe, and appear ideal candidates for this method. With proper care in preparation and cleaning of the electrode surfaces, we foresee that V_s can be made as small as a few tenths of a volt, rather than the 1.5 V observed here. Equation (5) provides a clear method for determining V_s from simple measurements of displacement, and greater stability in z should be achievable using the AFM scanner, where displacement noise can be less than a nanometer. With these considerations, it appears that SI traceable forces as small as 100 pN can be realized for AFM using the electrostatic force procedure, with relative uncertainties of a few percent. The chief obstacle to this application appears to be obtaining an AFM based electrode pair where V_s is stable to ± 5 mV.

[1] D. P. McDaniel, G. A. Shaw, J. T. Elliott, K. Bhadriraju, C. Meuse, K.-H. Chung, and A. L. Plant, Biophys. J. **92**, 1759 (2007).
[2] S. B. Smith, Y. Cui, and C. Bustamante, Science **271**, 795 (1996).
[3] D. Rugar, R. Budakian, H. J. Mamin, and B. W. Chui, Nature (London) **430**, 329 (2004).
[4] W. C. Oliver and G. M. Pharr, J. Mater. Res. **7**, 1564 (1992).
[5] M. R. VanLandingham, J. Res. Natl. Inst. Stand. Technol. **108**, 249 (2003).
[6] S. A. Syed Asif, K. J. Whal, and R. J. Colton, Rev. Sci. Instrum. **70**, 2408 (1999).
[7] J. R. Pratt, J. A. Kramar, D. B. Newell, and D. T. Smith, Meas. Sci. Technol. **16**, 2129 (2005).
[8] D. B. Newell, J. A. Kramar, J. R. Pratt, D. T. Smith, and E. R. Williams, IEEE Trans. Instrum. Meas. **52**, 508 (2003).
[9] R. S. Gates and J. R. Pratt, Meas. Sci. Technol. **17**, 2852 (2006).
[10] E. D. Langlois, G. A. Shaw, J. A. Kramar, J. R. Pratt, and D. C. Hurley, Rev. Sci. Instrum. **78**, 093705 (2007).
[11] G. A. Matei, E. J. Thoreson, J. R. Pratt, D. B. Newell, and N. A. Burnham, Rev. Sci. Instrum. **77**, 083703 (2006).
[12] P. J. Cumpson and J. Hedley, Nanotechnology **14**, 1279 (2003).
[13] J.-H. Choi, M.-S. Kim, Y.-K. Park, and M.-S. Choi, Appl. Phys. Lett. **90**, 073117 (2007).
[14] I. Behrens, L. Doering, and E. Peiner, J. Micromech. Microeng. **13**, S171 (2003).
[15] M.-S. Kim, J.-H. Choi, Y.-K. Park, and J.-H. Kim, Metrologia **43**, 389 (2006).
[16] This article is authored by employees of the U.S. Federal Government, and is not subject to copyright. Commercial equipment and materials are identified in order to adequately specify certain procedures. In no case does such identification imply recommendation or endorsement by the National Institute of Standards and Technology, nor does it imply that the materials or equipment identified are necessarily the best available for the purpose.
[17] *ZMI PC System Manual OMP-0434A* (Zygo, Middlefield, CT, 2000).
[18] *Andeen-Hagerling 2700A Ultra-precision Capacitance Bridge Operation and Maintenance Manual* (Andeen-Hagerling, Cleveland, OH, 2002).
[19] *Agilent Technologies 3458A Multimeter User's Guide*, 4th ed. (Agilent Technologies, Loveland, CO, 2001), Part No. 03458-90014.
[20] S. Hudlet, M. Saint Jean, C. Guthmann, and J. Berger, Eur. Phys. J. B **2**, 5 (1998).
[21] L. Kogut, J. Micromech. Microeng. **15**, 1068 (2005).
[22] J. R. Taylor, *An Introduction to Error Analysis* (University Science, Sausalito, 1997).
[23] F. Rossi and G. I. Opat, J. Phys. D **25**, 1349 (1992).
[24] J. B. Camp, T. W. Darling, and R. E. Brown, J. Appl. Phys. **69**, 7126 (1991).
[25] B. N. Taylor and C. C. Kuyatt, "Guidelines for evaluating and expressing the uncertainty of NIST measurement results," NIST Technical Note No. TN-1297, 1994.
[26] N. A. Seugling and J. R. Pratt, Proceedings of the ASPE Annual Meeting, Orlando, FL, 2004 (unpublished).